Sea Surface Temperature Estimation from the Geostationary Operational Environmental Satellite-12 (GOES-12)

Sea Surface Temperature Estimation from the *Geostationary Operational Environmental Satellite-12* (*GOES-12*)

C. J. MERCHANT

School of GeoSciences, University of Edinburgh, Edinburgh, United Kingdom

A. R. HARRIS AND E. MATURI

NOAA/NESDIS/Office of Research and Applications/Oceanic Research and Applications Division, Camp Springs, Maryland

O. EMBURY AND S. N. MACCALLUM

School of GeoSciences, University of Edinburgh, Edinburgh, United Kingdom

J. MITTAZ

NOAA/NESDIS/Office of Research and Applications/Oceanic Research and Applications Division, Camp Springs, Maryland

C. P. OLD

School of GeoSciences, University of Edinburgh, Edinburgh, United Kingdom

(Manuscript received 15 August 2007, in final form 13 August 2008)

ABSTRACT

This paper describes the techniques used to obtain sea surface temperature (SST) retrievals from the *Geostationary Operational Environmental Satellite 12* (*GOES-12*) at the National Oceanic and Atmospheric Administration's Office of Satellite Data Processing and Distribution. Previous SST retrieval techniques relying on channels at 11 and 12 μm are not applicable because *GOES-12* lacks the latter channel. Cloud detection is performed using a Bayesian method exploiting fast-forward modeling of prior clear-sky radiances using numerical weather predictions. The basic retrieval algorithm used at nighttime is based on a linear combination of brightness temperatures at 3.9 and 11 μm. In comparison with traditional split window SSTs (using 11- and 12-μm channels), simulations show that this combination has maximum scatter when observing drier colder scenes, with a comparable overall performance. For daytime retrieval, the same algorithm is applied after estimating and removing the contribution to brightness temperature in the 3.9-μm channel from solar irradiance. The correction is based on radiative transfer simulations and comprises a parameterization for atmospheric scattering and a calculation of ocean surface reflected radiance. Potential use of the 13-μm channel for SST is shown in a simulation study: in conjunction with the 3.9-μm channel, it can reduce the retrieval error by 30%. Some validation results are shown while a companion paper by Maturi et al. shows a detailed analysis of the validation results for the operational algorithms described in this present article.

1. Introduction

The National Oceanic and Atmospheric Administration's Office of Satellite Data Processing and Distribution has generated operational sea surface temperature (SST) retrievals from the Geostationary Operational Environmental Satellites (GOES) since December 2000. There are two platforms: GOES-E, situated at longitude 75°W; and GOES-W at 135°W. Geostationary orbit allows for the acquisition of high temporal resolution SST retrievals. The geostationary sensor provides thermal IR radiance data of sufficient precision to permit the retrieval of SST with accuracy approaching that of polar-orbiting

Corresponding author address: Dr. C. J. Merchant, School of GeoSciences, University of Edinburgh, Crew Building, King's Buildings, Edinburgh EH9 3JN, United Kingdom.
E-mail: chris@staffmail.ed.ac.uk

DOI: 10.1175/2008JTECHO596.1

sensors. The GOES SST products generated from these algorithms include hourly regional sectors, 3-hourly hemispheric imagery, and 24-h merged composites.

Since 2000, GOES SST has become the most requested NOAA satellite product for the U.S. coastal user community. The datasets have been invaluable for a wide range of environmental studies, including coastal and open ocean fisheries, climate, numerical weather prediction (NWP), and ocean and high seas forecasting. The accurate GOES SST data allows the climate community users to account for the diurnal SST effects.

GOES-12 became the operational GOES-E platform on 1 April 2003, replacing the ageing *GOES-8*. The latter was the original three-axis GOES platform launched in 1994. The *GOES-8*, *-9*, and *-10* imager, with three infrared channels (3.9, 11, and 12 μm), required a significant investment of resources over several years to generate SST products approaching Advanced Very High Resolution Radiometer (AVHRR)-like quality. Because the *GOES-12* satellite imager has only two channels (3.9 and 11 μm) available to generate SSTs, this heritage could not be directly transferred. The 3.9-μm channel is difficult to use during the day because of solar contributions to the signal that derive from surface reflection and atmospheric scattering. The *GOES-12* algorithm required a substantial departure from current operational methodology to ensure continued availability of daytime GOES SST retrievals. Continuity of operations required the generation of *GOES-12* SSTs for the numerous users of these products. This paper describes the *GOES-12* SST algorithms developed for operational implementation from 1 April 2003, including subsequent improvements to the processing function. Centers other than NOAA have generated GOES SST products operationally (May and Osterman 1998; Brisson et al. 2002) but, to our knowledge, no others are attempting to derive daytime SST products for *GOES-12* in the absence of the 12-μm channel.

2. *GOES-12* imager

The main difference for the purpose of this paper between the *GOES-12* imager and previous instruments in the series is that it is the first to have a channel at 13.3 μm. The spectral response of this channel falls in the wing of the strong CO_2 absorption band centered at 15 μm and the channel is, therefore, primarily sensitive to temperatures in the lower troposphere. This additional information is used to improve the height assignment of cloud-track winds (especially for subpixel and semitransparent clouds) via the CO_2-slicing approach. However, this new channel has replaced the one centered at 12 μm. The 12-μm channel is a key component of the SST retrieval algorithm applied to data from previous GOES imagers, which used the 3.9-, 11-, and 12-μm channels at night and is critically dependent on just the 11- and 12-μm channels for the daytime product. Given the success of the GOES SST product, it is highly desirable to establish a new scheme for continuing its production using the revised imager specification, especially since a 12-μm channel will not be available until GOES-R, which is currently scheduled for launch in 2012.

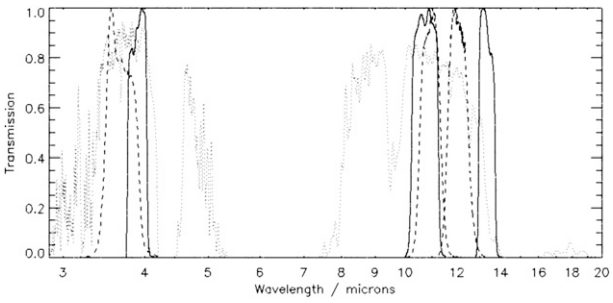

FIG. 1. Spectral responses and atmospheric spectral transmission. Dotted line indicates transmission for the std Michelson Interferometer for Passive Atmospheric Sounding (MIPAS) midlatitude atmosphere (available online at http://www-atm.physics.ox.ac.uk/RFM/rfm_downloads.html). Solid line indicates normalized spectral response functions for *GOES-12* channels. Dashed line indicates normalized spectral response functions for ATSR-2 channels.

Figure 1 shows the normalized spectral response functions of *GOES-12* channels at "3.9," "11," and "13" μm [together with those for a typical polar-orbiter channel set, in this case the Along-Track Scanning Radiometer-2 (ATSR-2) at "3.7", "11" and "12" μm] with the atmospheric transmittance for midlatitude conditions. The sensitivity of *GOES-12*'s 13-μm channel to surface temperature is small, given the low channel-integrated nadir transmittance of, typically, 0.3 (range of ~0.05–0.5).

3. Nighttime SST retrieval

a. Cloud detection

The first step in the retrieval of sea surface temperature using infrared imagery is the detection of image pixels whose radiances are significantly affected by the present of cloud in their field of view. The approach to cloud screening adopted for *GOES-12* operations is an implementation of the probabilistic, physically based method of Merchant et al. (2005). The reader is referred to Merchant et al. (2005) for a description of this method (and a brief review of alternative methods) and to the algorithm theoretical basis document for the details of the implementation for *GOES-12* (available from

NOAA/NESDIS/ORA/ORAD). The cloud-screening method is very briefly described in the remainder of this subsection.

The *GOES-12* cloud detection is based on the forward modeling of the expected observations and their error covariance, followed by the application of a formulation of Bayes' theorem to generate an estimate of the probability that each pixel is cloud free given the actual observations. The approach is, thus, explicitly formulated to match the underlying nature of the cloud detection problem. Cloud detection is always an attempt to assess the likelihood of an observation being cloud-free, given both the observation itself and prior information about the nature of both cloud-free and cloudy observations. Often the prior information is embedded, perhaps somewhat obscurely, in the thresholds of the various cloud screening tests applied. In our ''Bayesian'' approach, the prior information being used is made explicit, which makes the approach general and maintainable. Moreover, we benefit from being able to derive this prior information from forecast fields available within an operational center for numerical weather prediction.

NWP forecast fields (surface temperature and wind speed, and temperature and water vapor profiles) are used as input to the Community Radiative Transfer Model (CRTM) to predict the clear-sky brightness temperatures (BTs) at 3.9 and 11 μm and their error covariance for each pixel in the image. This error covariance includes the effect of sampling error from the mismatch in scale between the prior surface temperature field (on the model grid) and the pixel resolution observations. The predicted brightness temperatures and their error covariance define a joint Gaussian clear-sky brightness temperature probability distribution for the observations [refer to Merchant et al. 2005, their Eq. (6)].

The nighttime observation vector used for cloud detection also includes the local standard deviation (LSD) of both brightness temperatures across a 3 $\times$ 3 box centered on each pixel; the ''forward model'' for the LSD is a combination of the contribution to clear-sky LSD expected from radiometric noise (uncorrelated between channels) and the contribution from any frontal SST gradient in the vicinity of the pixel. The presence of a front of strength dT_s/dx (where T_s is SST and x is distance perpendicular to the front) can be shown to cause an LSD in a 3 $\times$ 3 box of pixels with ground resolution l of approximately

$$\sqrt{\frac{3}{4}}\frac{dT_s}{dx}l\frac{\partial T_\lambda}{\partial T_s}, \qquad (1)$$

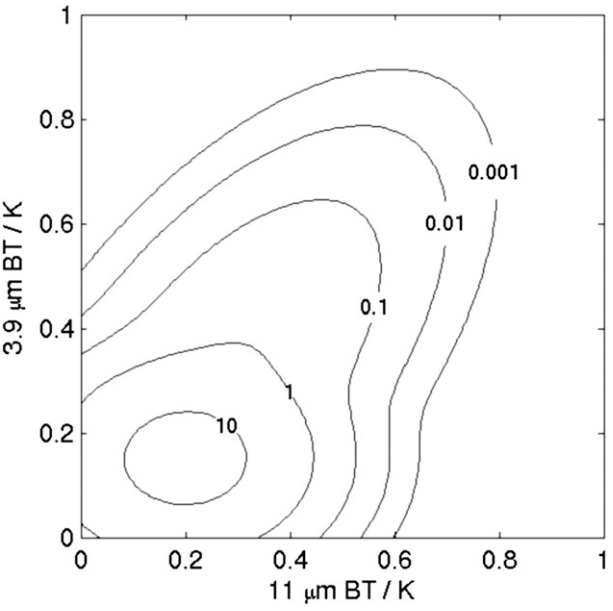

FIG. 2. Contours of probability density (K^{-2}) of LSD of *GOES-12* BTs across a 3 $\times$ 3 pixel box, assuming radiometric noise of 0.15 at 3.9, 0.20 K at 11 μm, and a 10% probability of a front of strength 0.15 K km^{-1}.

independent of the orientation of the front relative to the image pixels. Here, T_λ is the channel brightness temperature, with the channel wavelength λ being either 3.9 or 11 μm. The LSD from such a front is correlated between the channels. At present, the probability of a front being present and the strength of any such front are set to global constants. The obvious refinement of updating these parameters in the light of recent high-resolution SST analyses has yet to be explored and implemented, and one of the difficulties being faced is that frontal features in high-resolution SST products are not, in general, consistently reproduced and are subject to artifacts from some analysis procedures (e.g., those available online at www.mersea.eu.org/Satellite/sst_validation_l4_glob_oi.html). Fig. 2 shows an example of the joint LSD distribution obtained for *GOES-12* by the above means.

The probability density functions describing the distribution of brightness temperatures and LSDs of cloudy pixels are also required. At present, globally fixed distributions are used, which are shown in Fig. 3. These have been derived from cloud-flagged observations of 3.7- and 11-μm brightness temperatures in 1-km resolution images of the ATSR-2, aggregated up to 5-km boxes and with added synthetic radiometric noise, to be more representative of the *GOES-12* imager resolution and noise levels. The variability in cloudy brightness temperatures is large compared to the differences in

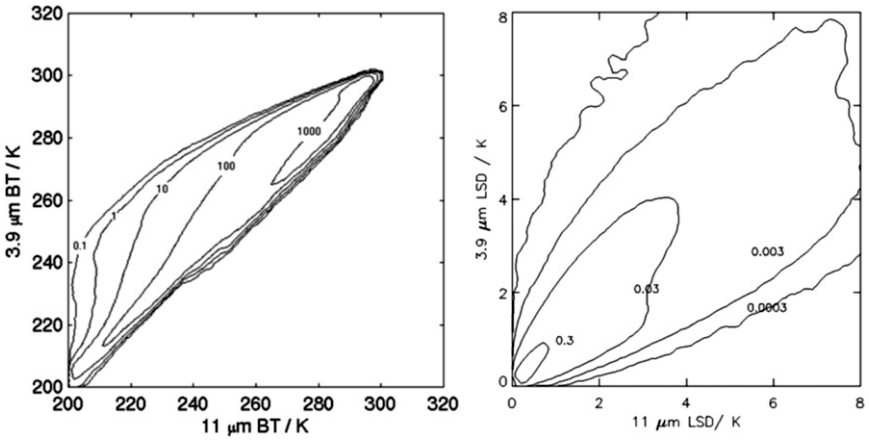

FIG. 3. Joint probability density functions for (left) BT and (right) LSD used to represent cloudy observations of the *GOES-12* imager. Lines are contours of (left) $10^6 \times$ probability K^{-2} of observing a given pair of BT, and (right) probability K^{-2} of observing a given pair of LSDs.

brightness temperatures arising from the different spectral responses of ATSR-2 to *GOES-12* (Fig. 1), so that using the ATSR-2-based probability density function for *GOES-12* screening performs adequately well. *GOES-12* specific probability density functions based on radiative transfer modeling are under development and being tested at the time of this writing.

We have described above how we define probability density functions for brightness temperatures and local standard deviation. Together with the actual brightness temperatures and local standard deviation, Bayes' theorem states how to estimate the probability of the location being clear sky. The output of the cloud detection step is, therefore, a probability of being clear sky for each pixel. A single threshold can now be defined to create a cloud mask, namely, the threshold of probability of clear below which we mask the pixel (i.e., do not calculate an SST). If the priority is to make the SST estimates accurate, we can be conservative and set this threshold at a high level (close to 1.0). If the priority is to avoid major cloud contamination while maximizing the area for which reasonable SST estimates can be formed, we can be lax and set the threshold relatively low (e.g., at 0.5). At present, we use a threshold of 0.8 (i.e., SST is not calculated for pixels below this probability). The most accurate SST retrievals are expected to be obtained for probabilities closest to 1.0, and the probability is retained as part of the SST product to satisfy users with different accuracy/coverage requirements. The Bayesian probability is also used, therefore, to define a "proximity confidence value" that ranks SSTs obtained into five quality categories, consistent with the framework of the Global Ocean Data Assimilation Experiment high-resolution SST pilot project (Donlon et al. 2007). For details of the interaction of this threshold and statistics on the validation of *GOES-12* SST, refer to the companion paper by Maturi et al. (2008).

b. Sea surface temperature estimation

The main novelty of the *GOES-12* imager from the viewpoint of SST estimation is the replacement of one of the traditional "split window" channels (at 12 μm) with a 13.3-μm channel (see section 2). The operational nighttime SST retrieval, therefore, uses only the 3.9- and 11-μm channels.

Linear split window estimators rely on the approximate proportionality of the atmospheric effect on brightness temperatures between channels at 11 and 12 μm. The main absorbing gas for split window channels is water vapor, and the proportionality between the channels is least strict at high water vapor loadings when the atmospheric transmittance in the 12-μm channel approaches zero. Split window estimators of SST, therefore, tend to be noisiest at high atmospheric water vapor loadings. Because of the latitudinal correlation of SST and atmospheric water vapor, it is broadly the case that split window SSTs tend to be noisiest where SSTs are warmest. Furthermore, the dependence of the proportionality between $T_s - T_{11}$ and $T_s - T_{12}$ on water vapor means that linear split window estimators have bias trends that are also generally related to scene temperature.

SST retrieval estimators using the 3.9- and 11-μm channels have a somewhat different characteristic, as shown in Fig. 4: the greatest scatter tends to be at lower SSTs. Figure 4 is based on the radiative transfer simulations undertaken for defining *GOES-12* retrieval coefficients for SST. NWP data from all seasons and times of day were sampled at the locations shown in Fig. 5 and

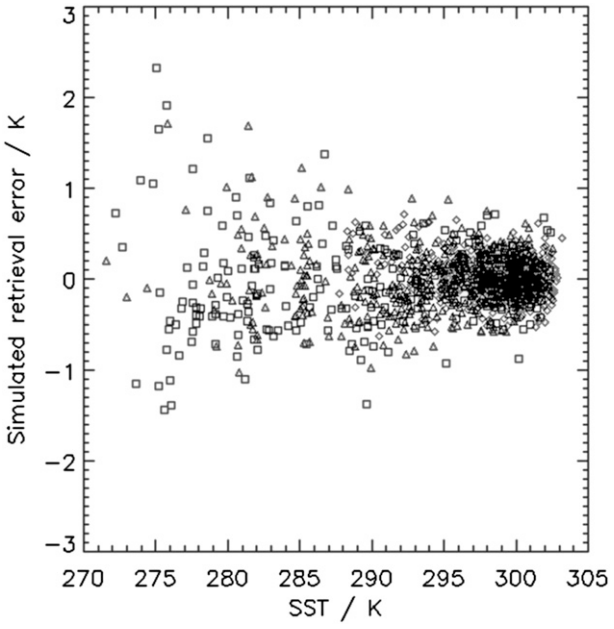

FIG. 4. Simulations of error in *GOES-12* 3.9-/11-μm SST retrievals plotted against SST. Diamonds indicate satellite zenith angles below 40°; triangles indicate zenith angles between 40° and 60°; and squares indicate zenith angles between 60° and 70°.

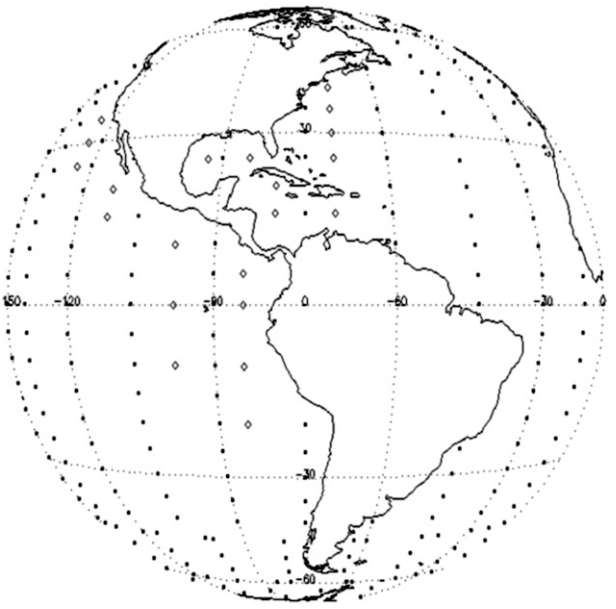

FIG. 5. Geometry of simulations for RTM for defining *GOES-12* retrieval coefficients. NWP profiles are obtained according to the sampling strategy of Merchant et al. (1999; squares), with some additional sampling in key areas (diamonds).

were used as inputs to the Moderate Spectral Resolution Atmospheric Transmittance (MODTRAN4) radiative transfer model run at 1 cm^{-1} spectral resolution to calculate brightness temperatures for *GOES-12* channels at the appropriate satellite zenith angle. The formulation of the SST estimator is

$$\hat{T}_s = a_1 + a_2 F_\theta + (a_3 + a_4 F_\theta) T_{3.9} + (a_5 + a_6 F_\theta) T_{11}, \quad (2)$$

where $F_\theta = \sec(\theta) - 1$, θ is the satellite zenith angle, and the a_i are the ''retrieval coefficients'' found by linear regression. Their values are $a_1 = -2.09$, $a_2 = 1.15$, $a_3 = 1.177$, $a_4 = 0.073$, $a_5 = -0.162$, and $a_6 = -0.069$. Errors in the characterization of sensor spectral response can lead to the retrieval coefficients based on the radiative transfer being suboptimal. As discussed in Merchant and Le Borgne (2004), such errors seem, in practice, principally to affect the bias of the retrievals such that the offset coefficient a_1 requires adjustment in the light of validation data. Figure 4 was then created by applying the retrieval coefficients back to a similar but independent set of simulated brightness temperatures with the added noise representative of *GOES-12*. The overall simulated retrieval error in Fig. 4 is 0.36 K. The increased scatter at lower SSTs arises as follows. The heaviest weight among the retrieval coefficients is on $T_{3.9}$ because it is the channel for which transmittance is higher and less variable (less sensitivity to water vapor). Variability in $T_s - T_{3.9}$ is more strongly influenced by the temperature of the atmosphere than $T_s - T_{11}$ because dry-air absorption (mainly from CO_2) is more significant, particularly when water vapor loadings are low. Therefore, $T_s - T_{11}$ can correct only part of the variability in $T_s - T_{3.9}$. In the tropical regions of high SST, the atmospheric and surface temperatures are tightly coupled, with air–sea temperature differences varying relatively little. In middle and high latitudes, the coupling of atmospheric and surface temperatures is less tight, with a wider range of air–sea temperature difference, stronger near-surface inversions, and more variable lapse rate. Therefore, the uncorrectable variability in $T_s - T_{3.9}$ tends to be greater in the middle and high latitudes where the surface temperature is low.

In the *GOES-12* products associated with each SST retrieval is a (pseudo) random retrieval error estimate that varies from pixel to pixel. This error estimate is formulated as

$$\varepsilon_{\mathrm{SST}} = \sqrt{(w_{3.9}\varepsilon_{3.9})^2 + (w_{11}\varepsilon_{11})^2 + (\varepsilon_{\mathrm{RET}})^2}, \quad (3)$$

where $w_{3.9} = a_3 + a_4[\sec(\theta) - 1]$ and $w_{11} = a_5 + a_6[\sec(\theta) - 1]$, they are obtained from the retrieval of Eq. (2). The assumed noise equivalent differential temperatures (NEdTs) in the two channels are $\varepsilon_{3.9} = 0.15$ and $\varepsilon_{11} = 0.20$ K. (An obvious refinement is to make these NEdTs depend on brightness temperature, since

the same radiometric noise is equivalent to a larger NEdT at colder temperatures because of nonlinearity in the Planck function, especially at 3.9 μm.) Here, $\varepsilon_{\mathrm{RET}}$ is an estimate of the intrinsic retrieval error associated with the formulation of the SST estimator. At present a single global value is assumed, derived from the global standard deviation of the scatter evident in the retrieval simulations shown in Fig. 4; the evident dependence of the standard deviation on SST is not parameterized in $\varepsilon_{\mathrm{RET}}$ at present. The other comment to make about $\varepsilon_{\mathrm{RET}}$ is that it is representing errors that are not wholly random. Day-to-day changes in surface and atmospheric state do cause associated errors in retrieved SST that appear random but which have nonzero mean in a longer-term average. In other words, there are systematic errors that contribute to the retrieval error, which Merchant et al. (2006) have identified as ''prior'' and ''nonlinearity'' error; the most significant characteristic for SST estimation of these forms of error is that they contribute bias that varies geographically and seasonally. The prior error is associated with the climatological difference between the state and the average state implicit in the regression data from which coefficients are derived (whether these data are based on radiative transfer modeling or empirical matches). The nonlinearity error is the inability of any linear or simple nonlinear SST estimator to capture the nonlinearity in the relationships between state and observations. Merchant et al. (2006) identified that these forms of bias can be estimated by detailed forward modeling. It has been common practice to ignore the mix of random and systematic error when discussing SST validation studies and in making SST retrieval error estimates. The approach described above for pixel-by-pixel error estimation within the *GOES-12* operations is a step toward refining the products supplied operationally to reflect the known variable characteristics of SST error, with a view toward improving the service provided particularly to sophisticated users, such as centers for data assimilation.

Refer to Maturi et al. (2008) for an assessment of the performance of the current operational *GOES-12* SST and the influence of air–sea temperature difference on retrieval errors.

4. Daytime SST retrieval

a. Solar contamination in the 3.9-μm channel

Estimating SST from daytime imagery of *GOES-12* is challenging compared to doing so from nighttime imagery and from the daytime imagery of earlier GOES imagers with a 12-μm channel. This is because, in the absence of a 12-μm channel, the channel at 3.9 μm has to be used, despite it containing potentially significant contributions to its radiance from scattered and reflected solar irradiance. (Use of the 11- and 13-μm channels together for SST retrieval was explored by radiative transfer simulation, giving a simulated SST retrieval error of 1.7 K, which is not a useful precision. Retrieval of SST with 11- and 12-μm relies on the fact that these two channels are differentially sensitive to essentially the same atmospheric parameters. This is not true of the combination of 11 and 13 μm.)

We deal with the solar contamination of the 3.9-μm channel by attempting to estimate and remove the solar contribution to radiance before undertaking cloud screening and SST estimation—we create a ''pseudonighttime'' $T_{3.9}$ image. As will be shown below, there is limited precision to which the solar contamination can be corrected. Quantitative correction, and cloud screening and retrieval are, therefore, only undertaken away from the main area of sun glint.

The pseudonighttime $T_{3.9}$ is formed by correcting for the effects of atmospheric scattering and sun glint. These corrections also have error estimates associated with them that are propagated into the cloud screening and SST retrieval, in addition to the estimated radiometric noise.

The radiance in the 3.9-μm channel is estimated using a parameterization based on the following considerations: (i) the number of scattering particles in the atmosphere viewed by the satellite is proportional to the pathlength at the satellite zenith angle, that is, to $\sec(\theta)$; (ii) the transmittance of the solar irradiance in passing through the atmosphere from sun to surface satellite is $\tau^{(\sec\theta + \sec\vartheta)}$, where τ is the global mean nadir transmittance and θ is the solar zenith angle. We fitted the parameters b_{i} ($i = 1, \ldots, 3$) in an equation for the path-scattered solar radiance observed by the sensor L_{scat}:

$$L_{\mathrm{scat}} = (b_1 \sec\theta) b_2^{(\sec\theta + \sec\vartheta)} + b_3. \qquad (4)$$

This solar radiance was simulated by MODTRAN4, assuming marine-type aerosols, and using a surface meteorological visibility of 10, 23, and 50 km. The locations of simulation were as before, with each location being run with the sun at several elevations above the horizon. The performance of the parameterization in simulation is illustrated in Fig. 6a, for the case of a surface meteorological visibility of 23 km. Despite its simplicity, the parameterization captures a significant proportion of the variance (40%) in the 3.9-μm brightness temperature difference associated with solar radiance scattered in the atmosphere into the *GOES-12* line of sight. The error in the estimate of the change in brightness temperature is 0.37 K. For the smaller

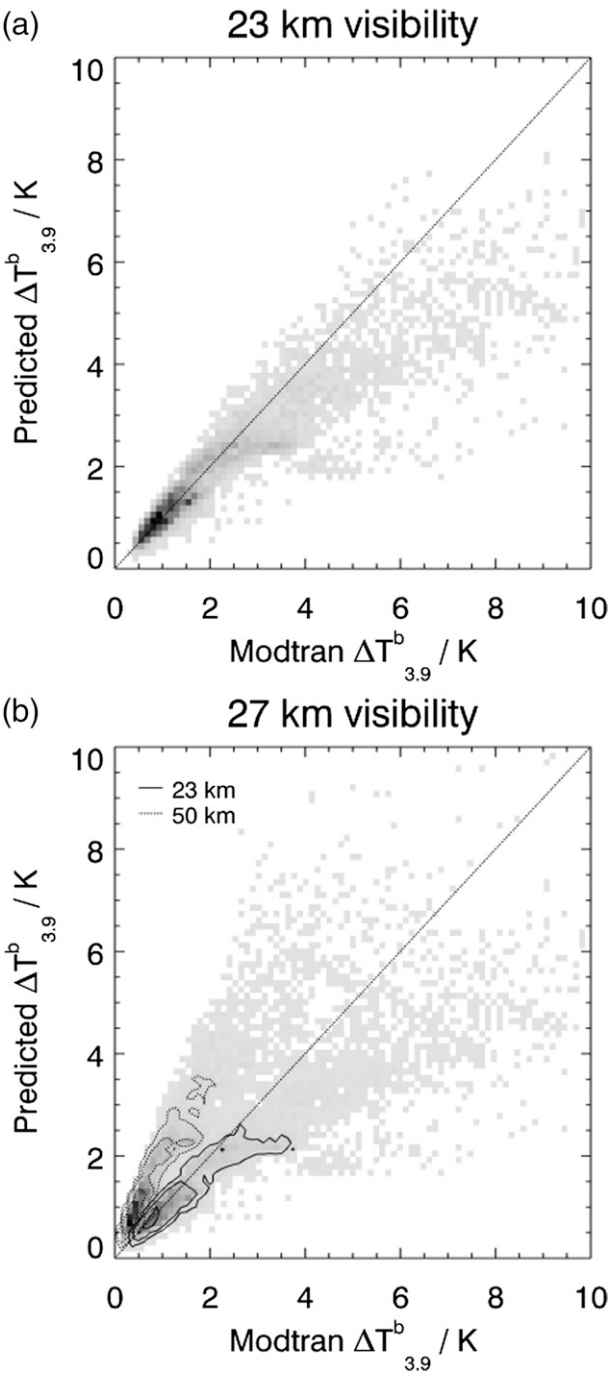

FIG. 6. Parameterization of effect of path-scattered radiance on the 3.9-μm channel BT. (a) Scatterplot of parameterized estimates (predicted ΔT_b) against effect fully simulated by MODTRAN4 (Modtran ΔT_b) for surface meteorological visibility of 23 km. Darker squares indicate a greater density of points within the square. (b) Same as in (a), but with a fixed 27-km visibility assumed for the predicted values against MODTRAN4-simulated values for visibilities of 50 (distribution with dotted contour lines) and 23 km (distribution with solid contour lines).

changes, up to 1.5, the error is 0.25 K, capturing 47% of the variance.

Given a prior estimate of surface meteorological visibility, the coefficients for the three precalculated visibilities can be interpolated with respect to the reciprocal of the prior visibility. However, the operational code at present assumes a fixed visibility of 27 km. As is evident from Fig. 6b, there is a significant dependence on the visibility that could be addressed by using an operational prior. More generally, this parameterization does not account for any azimuthal dependence of scattering, and it does not use prior information about atmospheric transmittance; therefore, it is somewhat limited and is in fact a temporary expedient. Once a fast radiative transfer model is available operationally that includes scattered solar radiance at 3.9 μm, the parameterization will be superseded.

In addition, it is necessary to estimate the solar radiance reflected by the surface of the ocean into the sensor's view. This is calculated as

$$L_{\text{refl}} = \left[\frac{\rho(\omega)\sec^4(\theta_n)\,P(z_x, z_y)}{4\cos(\theta)}\right] \times \Omega_{\text{SUN}} \times L_{\text{SUN}} \times \tau, \tag{5}$$

where $\rho(\omega)$ is the water reflectivity, which depends on the angle of incidence ω to glinting facets of the water surface; θ_n is the facet normal at the point of reflection; $P(z_x, z_y)$ is the probability of facets oriented with θ_n given the upwind (z_x) and crosswind (z_y) slopes of the glinting facets; Ω_{SUN} is the solid angle subtended by the sun; L_{SUN} is the solar radiance integrated over the 3.9-μm channel, 230.6 W m^{-2} str^{-1}; and τ here is the two-way transmittance of the atmosphere. We derive the water reflectivity from Hale and Querry (1973), and the facet slope probability density function is that of Cox and Munk (1954), which is parameterized in terms of 12.5-m wind speed.

The radiances with the L_{refl} contribution subtracted are converted to brightness temperature changes using the channel-integrated radiance-to-brightness temperature relationship, the difference between these and the radiance not so adjusted being ΔT_{GLINT}. The sun-glint effect on SST is then calculated as

$$\Delta T_s = \left\{a_3 + a_4[\sec(\theta) - 1.0]\right\} \times \Delta T_{\text{GLINT}} \tag{6}$$

and a "valid" pseudonighttime $T_{3.9}$ is only estimated if this evaluates to less than 1.0 K, since the error in ΔT_{GLINT} is estimated as 20% and stronger glint will degrade the SST retrieval significantly. Figure 7 illustrates the magnitude and extent of ΔT_{GLINT} (by showing the spatial distribution of $T_{3.9}$–T_{11}, which is dominated by the effect of solar contamination in the glint region)

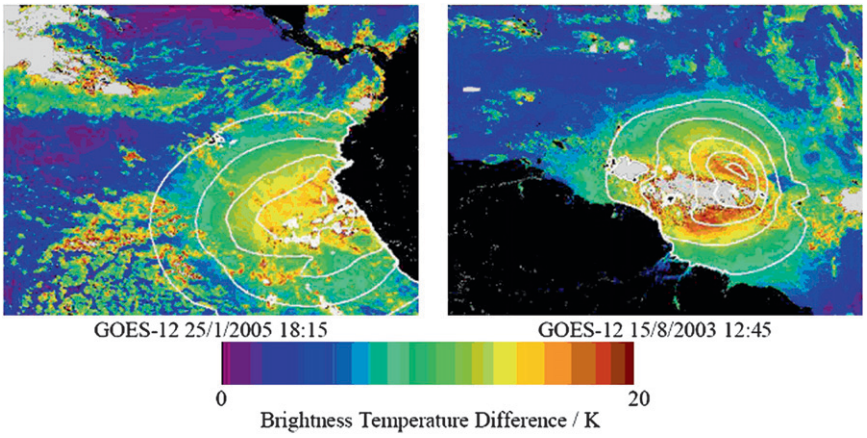

FIG. 7. BT at 3.9 μm minus that at 11 μm for two extracts from *GOES-12* imagery, with dates and times as indicated. Areas of large positive difference are associated with elevated BT in the 3.9-μm channel from sun glint (near-circular areas) and/or reflection from clouds (mottled features). Black areas are land-masked areas of Central and South America; gray areas are off scale (difference exceeding 20 K). Overlaid are contours of estimated change in 3.9-μm BT due to glint.

and examples of the 1-K contour outside of which a valid pseudonighttime $T_{3.9}$ is considered valid.

b. Daytime cloud screening

The daytime cloud screening is based on an observation vector comprising the visible reflectance (channel 1 of the imager), the 11-μm brightness temperature, the LSD of the visible reflectance, and the LSD of the 11-μm brightness temperature. At present, a simple analytic parameterization of the visible reflectance of the ocean under clear sky is used as the forward model for channel 1. This involves parameterizing the overall ocean albedo in terms of solar zenith angle and then applying an anisotropy function (e.g., Kidder and Vonder Haar 1995) to the albedo to estimate the observed reflectance; the anisotropy function is a function of satellite and solar zenith angles and of their relative azimuth angle. Given that atmospheric variability and ocean roughness are not considered, the estimated error is 50%, which is sufficient given the typically large ratio between clear-sky and cloudy-sky reflectance and allows for normal variations in marine aerosols. We assume a uniform frequency distribution of cloudy-sky reflectance. The distribution of the local standard deviation of the clear-sky visible reflectance is based on estimated instrumental noise alone, that is, it is assumed that real reflectance variations over length scales of three pixels are negligible for clear-sky ocean. The distribution of the LSD of the cloudy-sky visible reflectance is assumed to be uniform between 0% and a maximum value; this maximum value is calculated for a hypothetical extreme situation in which three pixels within the 3 $\times$ 3 box have 100% reflectance and the remainder have 0% reflectance. Given that that is a maximum reflectance contrast and that the assumption of complete filling or nonfilling of pixels is extreme, this provides a sensible maximum for LSD. The above set of assumptions and approximations are sufficiently effective to be employed in this first-generation algorithm but are not the optimum representation. Because the Bayesian approach decomposes the problem of cloud detection into specifying these distributions, the way in which we will obtain further improvements in cloud detection is clear: we will increase the realism of the distributions for visible reflectance and its local standard deviation.

c. Sea surface temperature estimation

The same retrieval Eq. (2) is used for daytime SST estimation as it is for nighttime but with the pseudonighttime $T_{3.9}$ replacing the actual 3.9-μm brightness temperature. For the SST retrieval error estimate, the NEdT for the 3.9-μm channel is augmented by an independent error in the solar radiance correction, estimated to be 20% of the correction at nadir and rising to 100% of the correction at a satellite zenith angle of 80° (i.e., typically less than 0.5 K but up to a few kelvin in unfavorable configurations).

5. Ongoing developments

a. Cloud detection

The operational cloud detection code for GOES SST operations was the first implementation of the Bayesian screening approach outlined by Merchant et al. (2005). An ongoing project (Mackie et al. 2008, manuscript

submitted to *Int. J. Remote Sens.*) is developing a modular, generic implementation of cloud detection software based on this approach, which will become the operational GOES SST cloud detection in the near future. This software library will also be generally and freely available under a public license. Within that framework, the future development of the cloud detection algorithms will involve two improvements. First, when the functionality of the CRTM is expanded to cover fast forward modeling of the GOES visible-channel transmittance, we will replace the albedo-based forward model for visible reflectance with the CRTM and the surface reflectance model based (as with the glint correction estimate) on forecast winds. Second, and more tentatively, we will assess the use of the 13-μm brightness temperature available with *GOES-12* for Bayesian cloud detection. The 13-μm channel is designed to assist height determination of cloud tops, and thus includes cloud information in its signal; however, in terms of mere cloud detection (as opposed to cloud parameter retrieval), the added information it brings remains to be assessed.

b. SST estimation

In section 4b, we discussed the characteristics of SST retrieval using the 3.9- and 11-μm channels. The question arises as to whether the 13-μm channel, not traditionally used for SST, has any useful information content for SST estimation. The 13-μm channel is sensitive to the temperature of tropospheric carbon dioxide, as, to a smaller degree, is the 3.9-μm channel. This differential sensitivity to, in effect, air–sea temperature difference and lapse rate implies some potential for the former channel to add useful information about an aspect of the atmospheric correction in the latter channel. This is borne out in simulations of SST retrieval error using the three-channel combination 3.9, 11, and 13 μm, as shown in Fig. 8. The retrieval accuracy is particularly improved in the cold, low-water vapor regime, where the 3.9- /11-μm algorithm displays most scatter for reasons already outlined in section 3b. The overall simulated retrieval error is reduced from 0.36 to 0.23 K by adding the 13-μm channel. In brief, it appears that, in validation, the scatter of estimated SST is reduced by introducing the 13-μm channel. However, a large bias is present, and it appears that significant radiance bias correction (relative to our forward modeling configuration) of the 13-μm channel will be required before operational exploitation can occur. (As an aside, we can comment that, in simulation studies, using a 13-μm channel for SST in addition to the usual suite of SST channels at 3.9, 11, and 12 μm is found to *reduce* retrieval standard deviation by about 10%.)

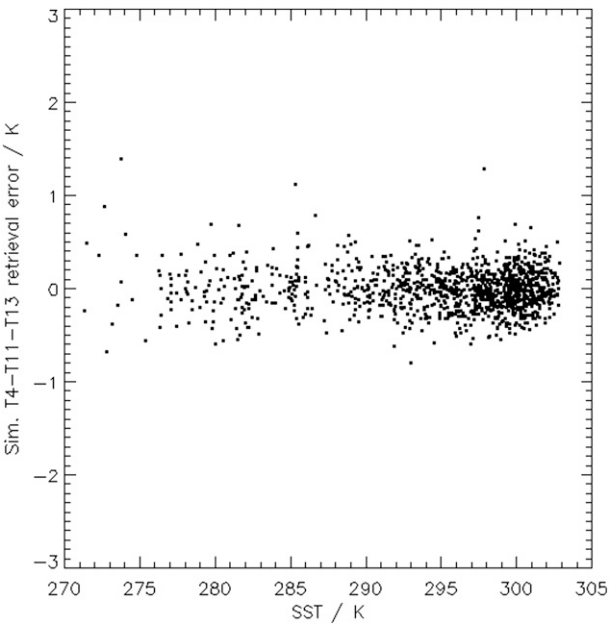

FIG. 8. Same as in Fig. 4, but for SST retrieval using 3.9-, 11-, and 13-μm channels together.

6. Summary validation results and conclusions

A detailed analysis of the performance of the retrieval methods described above is provided by the companion paper by Maturi et al. (2008). That paper extensively explores the relationships between biases in the SST retrievals and factors such as atmospheric state, zenith angle, and Bayesian probability of cloudiness, among others, and describes in detail the characteristics of the matchup database (MDB) used. Here, we present some summary validation results that are consistent with those analyses, presenting results for both *GOES-10* and *GOES-12*, to elucidate the effects of the absence of the 12-μm channel in the latter case.

Figure 9 shows distributions of *GOES-10* SST minus matched drifting buoy SSTs. The results are separated into night and day cases. Recall that for *GOES-10*, nighttime retrievals use three channels (3.9, 11, and 12 μm) and daytime retrievals use the split window channels (11 and 12 μm). The standard deviation (SD) of the distribution in Fig. 9a is 0.58 K, which is less than the comparable value for daytime SSTs (0.84 K), partly because of the extra information added by the 3.9-μm channel. For both day and night cases, there is a trend toward warm bias at low atmospheric correction (Figs. 9b and 9d), that is, at small values of the difference between the surface temperature and the 11-μm BT. This arises because of bias between the radiative transfer model (RTM) used to define coefficients and reality. Such bias can arise as a result of the lack of

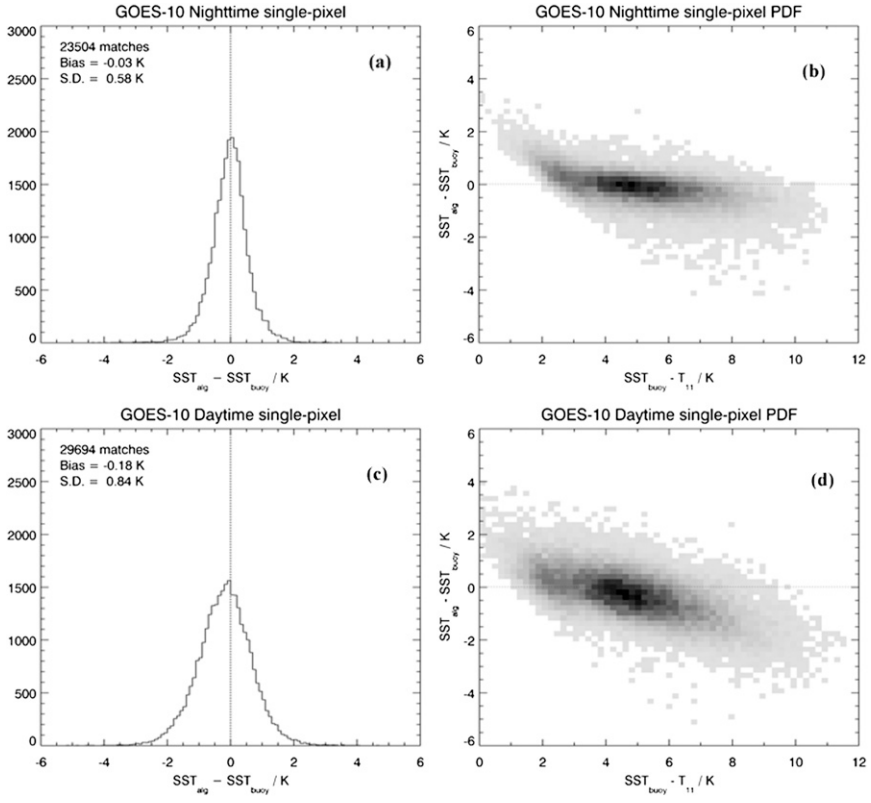

FIG. 9. Summary validation results for the *GOES-10* sensor. (a) Frequency distribution of retrieved minus drifting buoy SST, nighttime cases. (b) Distribution of difference of retrieved SST from drifting buoy SST against atmospheric correction at 11 μm. Density of shading reflects the relative population density of points, with >99% of points being in midgray to black areas. (c),(d) Same as in (a),(b), but for daytime cases.

realism of the atmospheric state assumed for the simulations because of biases within the RTM because of the error in the instrumental characterization provided to the RTM or because of other instrument calibration biases. Each of these can manifest as a trend relative to atmospheric correction because the effect of each bias source can be related to either atmospheric water vapor or scene brightness temperature, both of which correlate with atmospheric correction. Maturi et al. (2008) look at these possibilities in detail and deduce that instrument calibration and characterization errors are dominant and require radiance bias correction.

The corresponding results for *GOES-12* are shown in Fig. 10. The nighttime bias is −0.53 and the nighttime SD is 0.66 K (Fig. 10a). This SD is greater than the *GOES-10* equivalent, reflecting at least in part the lack of information from a 12-μm channel in the *GOES-12* SST based on 3.9 and 11 μm. To assess the intrinsic potential of *GOES-12* SST based on 3.9 and 11 μm, the coefficients were applied to an independent matchup database of nighttime matches from the Ocean and Sea Ice Satellite Application Facility (available online at http://www.osi-saf.org). Using the most conservative cloud masking category for this MDB (confidence level 5), the bias is −0.27 and the SD is 0.40 K. This SD is a significant improvement on the results in Fig. 10 and is more representative of the quality of the coefficients under conditions of clear skies, as determined by a stricter cloud mask.

Despite using the same retrieval coefficients, the daytime *GOES-12* SST has a broader SD of 0.89 K. This is partly the affect of having to use the pseudonighttime 3.9-μm BT (although there is also greater variability between SST measured at buoy depth and the skin SST during the day because of diurnal warming). The increased error in daytime *GOES-12* SSTs is reflected in the products' SST error estimates, as described above. The trend with atmospheric correction for nighttime data (Fig. 10b) is similar to that for *GOES-10*, whereas there is little trend for the daytime retrievals (Fig. 10d). This latter outcome must be somewhat fortuitous, since the retrieval equation is identical: a systematic effect in the correction of solar contamination happens to offset the trend that would otherwise be similar to that for nighttime.

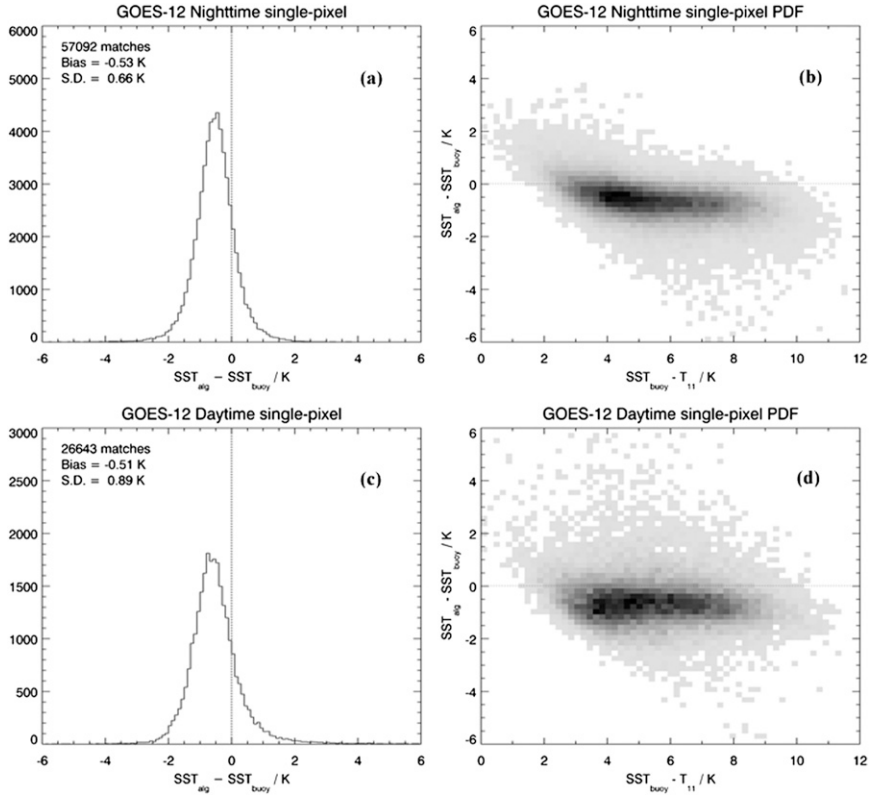

FIG. 10. Same as in Fig. 9, but for *GOES-12* SSTs.

There is a scattering of individual retrievals with errors exceeding +3 K, attributable to cases in which the correction of solar contamination has proved inadequate. While ''cold scatter,'' usually due to residual cloud contamination or excessive aerosol burden, is not uncommon in validation studies for single-view sensors, such ''warm scatter'' is a peculiarity of the *GOES-12* daytime. In the latter case, the atmospheric contaminant may serve to increase the scattered solar component of the 3.9-μm channel, which carries the highest weight in the retrieval [see the value of a_3 coefficient of Eq. (4) in section 3b].

GOES SST operations continue to develop with the aim of delivering improved products to users. There is, therefore, some difficulty in reporting in the scientific literature the techniques used because those techniques are evolving. Appropriately for an operational agency whose priority is the security of product supply to users, there is also a lag between devising improved techniques and implementing them operationally to allow for testing. In this article, we have, therefore, attempted to describe the key innovative elements of *GOES-12* SST as operationally produced at time of writing while fully acknowledging the limitations and approximations of the current approaches and indicating the directions that will be taken in future operational upgrades.

The main advance described herein is the development of an operational methodology for the production of SST from *GOES-12* imager data. This, in turn, has necessitated the development of algorithms for the retrieval of SST in the daytime using the 3.9- and 11-μm channels. Because the former channel is subject to contamination from scattered and reflected solar radiation, algorithms have been devised to correct for these error sources that are fast enough to serve in the operational context. Further changes have included the revision of the nighttime SST retrieval to function without the 12-μm channel, and the adoption of a probabilistic physically based cloud screening procedure. It should be noted that the new cloud detection scheme is applied to data from both operational GOES platforms. While it is recognized that the methodologies (particularly the correction for scattered solar radiation) are likely to require some enhancement, the validation results indicate that the SST product from *GOES-12* achieves useful accuracy, even in daytime. Nonetheless, the results are inevitably degraded compared to the *GOES-10* sensor. Finally, the product now includes the actual

probability of clear-sky estimates for each pixel, although a traditional masked version (currently thresholded at $P_{clear} = 0.98$) is also available to maintain continuity. This may be regarded as a first step in the development of added-value operational products for end users, which contain individual quantitative estimates of data accuracy for each pixel.

Acknowledgments. We thank Gerald Dittberner of the Office of Systems Development, Mark De Maria of GIMPAP, and Donald Gray of GOES-PSDI for providing the funding for this project. O Embury, C. P. Old, and S. N. MacCallum were funded by NOAA/NESDIS. A. Harris and J Mittaz were funded through the NOAA Cooperative Institute for Climate Studies. Special thanks to the NESDIS Office of Satellite Data Processing for their work in operationalizing this *GOES-12* SST product. The contents of this paper are solely the opinions of the authors and do not constitute a statement of policy, decision, or position on behalf of NOAA or the U.S. government. We thank the anonymous reviewers for helping us improve this manuscript and, in particular, the reviewer who applied *GOES-12* coefficients within the OSI-SAF MDB to generate a further point of comparison for the summary validation.

REFERENCES

Brisson, A., P. Le Borgne, and A. Marsouin, 2002: Results of one year of preoperational production of sea surface temperatures from *GOES-8*. *J. Atmos. Oceanic Technol.,* **19,** 1638–1652.

Cox, C., and W. Munk, 1954: Measurement of the roughness of the sea surface from photographs of the sun's glitter. *J. Opt. Soc. Amer.,* **44,** 838–850.

Donlon, C., and Coauthors, 2007: The Global Ocean Data Assimilation Experiment High-Resolution Sea Surface Temperature Pilot Project (GHRSST-PP). *Bull. Amer. Meteor. Soc.,* **88,** 1197–1213.

Hale, G. M., and M. R. Querry, 1973: Optical constants of water in the 200-nm to 200-μm. *Appl. Opt.,* **12,** 555–562.

Kidder, S. Q., and T. H. Vonder Haar, 1995: *Satellite Meteorology: An Introduction*. Academic Press, 466 pp.

Maturi, E. M., A. R. Harris, C. Merchant, J. Mittaz, B. Potash, W. Meng, and J. Sapper, 2008: NOAA's Geostationary Operational Environmental Satellites—sea surface temperature (GOES—SST) products. *Bull. Amer. Meteor. Soc.,* **89,** 1877–1888.

May, D. A., and W. O. Osterman, 1998: Satellite-derived sea surface temperatures: Evaluation of *GOES-8* and *GOES-9* multispectral imager retrieval accuracy. *J. Atmos. Oceanic Technol.,* **15,** 788–797.

Merchant, C. J., and P. Le Borgne, 2004: Retrieval of sea surface temperature from space, based on modeling of infrared radiative transfer: Capabilities and limitations. *J. Atmos. Oceanic Technol.,* **21,** 1734–1746.

——, A. R. Harris, M. J. Murray, and A. M. Zavody, 1999: Toward the elimination of bias in satellite retrievals of skin sea surface temperature. 1: Theory, modeling and inter-algorithm comparison. *J. Geophys. Res.,* **104** (C10), 23 565–23 578.

——, ——, E. Maturi, and S. MacCallum, 2005: Probabilistic physically based cloud screening of satellite infrared imagery of operational sea surface temperature retrieval. *Quart. J. Roy. Meteor. Soc.,* **131,** 2735–2755.

——, L. A. Horrocks, J. Eyre, and A. G. O'Carroll, 2006: Retrievals of sea surface temperature from infrared imagery: Origin and form of systematic errors. *Quart. J. Roy. Meteor. Soc.,* **132B,** 1205–1223.